ELSEVIER

Journal of the Neurological Sciences 216 (2003) 1–10

Journal of the Neurological Sciences

www.elsevier.com/locate/jns

Review article

Virtual and real brain tumors: using mathematical modeling to quantify glioma growth and invasion

Kristin R. Swanson[a,b], Carly Bridge[a], J.D. Murray[b], Ellsworth C. Alvord Jr[a,*]

[a] *Department of Pathology, University of Washington and Laboratory of Neuropathology, Harborview Medical Center, 325 9th Avenue, Box 359791, Seattle, WA 98104-2499, USA*

[b] *Department of Applied Mathematics, University of Washington, Box 352420, Seattle, WA 98195-2420, USA*

Received 19 March 2003; accepted 2 June 2003

Abstract

Over the last 10 years increasingly complex mathematical models of cancerous growths have been developed, especially on solid tumors, in which growth primarily comes from cellular proliferation. The invasiveness of gliomas, however, requires a change in the concept to include cellular motility in addition to proliferative growth. In this article we review some of the recent developments in mathematical modeling of gliomas. We begin with a model of untreated gliomas and continue with models of polyclonal gliomas following chemotherapy or surgical resection. From relatively simple assumptions involving homogeneous brain tissue bounded by a few gross anatomical landmarks (ventricles and skull) the models have recently been expanded to include heterogeneous brain tissue with different motilities of glioma cells in grey and white matter on a geometrically complex brain domain, including sulcal boundaries, with a resolution of 1 mm^3 voxels. We conclude that the velocity of expansion is linear with time and varies about 10-fold, from about 4 mm/year for low-grade gliomas to about 3 mm/month for high-grade ones.

Keywords: Glioma; Mathematical model; Tumor invasion; Tumor growth

1. Introduction

Gliomas are diffuse and highly invasive brain tumors accounting for about 50% of all primary brain tumors [1]. The prognosis for patients with gliomas depends on many factors, including the histologic type and grade of malignancy, the patient's age and level of neurological functioning [2]. However, the ''grade of malignancy'' includes at least two factors, net proliferation rate and invasiveness, that are estimated histologically but practically never defined accurately. Unlike solid tumors, for which simple exponential or geometric expansion represents expansion of volume (equivalent to the number of cells in the tumor), gliomas consist of motile cells that can migrate as well as proliferate. Indeed, the invasiveness makes it almost impossible to define the growth rate as a classical volume-doubling time, as Blankenberg et al. [3] attempted, even in the ideal case where at least two scans (CT, MRI) are analyzed at different times without treatment intervening. The boundary between tumor and normal tissue is not sharp and the number of cells in the ''normal tissue'' is not determinable. Clearly new mathematical formulations are necessary for gliomas since it is practically impossible either to measure the growth rate or to determine the spatio-temporal infiltration of gliomas necessary to apply the results of decades of investigations of mathematical formulations of other cancers.

Considering that the median untreated survival time for high grade gliomas ranges from 6 months to 1 year [1] and that even slowly growing gliomas can rarely be cured by radical resection, it seems clear that gliomas are in fact biologically malignant. In general, they are not encapsulated, and even apparently encapsulated ependymomas are not curable by simple resection [4]. These observations fit with the fact that individual glioma cells are highly motile, with the ability to invade most of the neural axis of rats in less than 1 week following implantation and are known to be viable even long distances from the bulk lesion in humans [5]. Additionally, gliomas can exhibit very high proliferation

* Corresponding author. Tel.: +1-206-731-6315; fax: +1-206-731-8240.

E-mail addresses: swanson@amath.washington.edu (K.R. Swanson), cbridge@u.washington.edu (C. Bridge), murrayjd@amath.washington.edu (J.D. Murray), alvord@u.washington.edu (E.C. Alvord).

0022-510X/$ - see front matter © 2003 Elsevier B.V. All rights reserved.
doi:10.1016/j.jns.2003.06.001

rates with doubling times ranging down to 1 week in vivo [1].

2. Why use mathematical models?

Mathematical modeling is a powerful tool for analyzing biological problems that allows one to develop and test hypotheses which can lead to a better understanding of the biological process. The essentials of a realistic and useful model are

(i) a sound understanding and appreciation of the biological problem;
(ii) a realistic mathematical representation of the important biological phenomena;
(iii) finding useful solutions, preferably quantitative; and what is crucially important,
(iv) a biological interpretation of the mathematical results in terms of insights and predictions. The mathematics is dictated by the biology and not vice-versa [6].

Of utmost importance to mathematical modeling, each of the variables in the mathematical formulation can be considered individually or together to assess their significance to the biological problem and to suggest hypotheses or conclusions that can be tested biologically. Upon comparison with real life results, the model can be modified to more accurately emulate the phenomena. This iterative process of calculating model results and making biological comparisons can continue to the point at which the model suggests appropriate experiments to clarify portions of the biological mechanism not yet understood and to make realistic predictions [6].

3. A brief history of mathematical modeling of tumor growth

Cancer research has been a fertile ground for mathematical modeling, beginning with the early concept of simple exponential growth of solid (usually benign) tumors doubling at a constant rate: 1 cell, 2 cells, 4 cells, 8 cells, ... This concept was actually found by Collins et al. [7] to apply also to malignant human tumors, specifically metastases studied by the simple technique of serial chest X-rays. Kusama et al. [8] then correlated the survival time following radical resection of breast cancers with the exponential growth rate. The introduction of logistic (gompertzian) growth allowed for the slowing of growth in the later stages as the tumor cells outgrew their blood supply, producing central necrosis. The ultimate simplification of this pattern, one actually found in a particular rat sarcoma [9], became linear mathematically as the thin surface of viable tumor cells surrounding the necrotic core grew essentially in only two dimensions. This was also applicable to simple epidermoid cysts [10].

With the recognition that tumor cells might spread outside the grossly visible mass, invading locally and/or metastasizing distantly, and that not all tumor cells are immortal, the mathematical concepts necessarily became more complicated than provided by the original simple models of solid tumors.

Deisboeck et al. [11] suggested that brain tumors behave as complex dynamic and self-organizing biosystems and used computer visualizations and simulations involving cellular automata and agent-based modeling and image processing techniques. This work has some application to cell cultures but has not yet been adapted to real gliomas in actual patients.

Experimental studies and theoretical analyses turned to cellular kinetics, in which the growth fraction and cell cycle kinetics (especially the S-phase of DNA synthesis and the rate of incorporation of tritiated thymidine and later bromodeoxyuridine) figured extensively. The pioneering work of Steel [12] led to many variations of flow cytometric analyses. With these studies it quickly became apparent that there was an order of magnitude difference between the times involved in the definitions of cellular and gross kinetics: hours to a few days for individual cells, many days and even months for gross tumors.

Steel [12] formulated some of these concepts into rather formidable equations involving potential and actual volume-doubling times, cell cycle and DNA-synthesizing times, mitotic and labeling indices, cell loss and growth fraction. Additional considerations of the amount of tumor left behind post-operatively spawned attempts to simplify these concepts into something more manageable. The recognition that 36.5 doublings of a 10-μm cell would produce approximately 100 g of tumor in 1 year if the volume-doubling time was 10 days led to the development of a simple nomogram [1]; simple, that is, if one accepts several oblique parallel lines superimposed on a double logarithmic background, all accommodating at least six labeled axes. This nomogram allowed approximate solutions to Steel's equations [12], but this was merely arithmetic manipulation and did not address the key question of how to measure the growth rate of an infiltrating glioma.

4. The mathematical model: interaction of migration and net proliferation

The initial answer to the question of how to measure the growth of an infiltrating glioma was provided by Professor J.D. Murray in the early 1990s. He formulated the problem as a conservation equation [6]. In words, this is written as follows:

$$\begin{aligned}&\text{the rate of change of tumor cell population}\\ &= \text{the diffusion (motility) of tumor cells}\\ &\quad + \text{the net proliferation of tumor cells.}\end{aligned} \tag{1}$$

Mathematically, the word equation (1) for untreated gliomas can be reasonably quantified by a single partial differential equation

$$\frac{\partial c}{\partial t} = \nabla \cdot J + \rho c$$

in which $c(\mathbf{x},t)$ designates the tumor cell density at location $\mathbf{x}$ and time t, ρ denotes the net proliferation rate, and ∇ defines the spatial gradient operator. Under the assumption of classical gradient-driven Fickian diffusion, $J = D\nabla c$, the model can be written

$$\frac{\partial c}{\partial t} = \nabla \cdot (D\nabla c) + \rho c \qquad (2)$$

where D is the diffusion coefficient representing the active motility of glioma cells. The model formulation is completed by boundary conditions which impose no migration of cells beyond the brain boundary and initial conditions $c(x,0) = f(x)$ where $f(x)$ defines the initial spatial distribution of malignant cells.

The original analyses of the model took the brain tissue to be homogeneous so that the diffusion coefficient D, defining random motility of the glioma cells, was constant and uniform throughout the brain [13–16]. Tumor growth is generally assumed to be exponential, so that the cell growth term, ρc, in the equation is a constant. However, logistic and gompertzian growth are also possible and have been considered but found to be unnecessary in the time frames considered for gliomas [13,14]. It was found, however, that there had to be two phases of growth, an early one without diffusion up to about 1 mm^3 before Eq. (2) becomes applicable; otherwise, gliomatosis cerebri developed without any bulk tumor growth apparent.

An interesting consequence of the basic model assumptions is that the profile of the concentration of tumor cells depends on the ratio of the growth rate ρ to the diffusion coefficient D. That is, varying ρ and D with ρ/D fixed, the geometry of the tumor growth and invasion remains the same, only the time scale on which the growth and invasion occurs is changed. Specifically, two different tumors with ρ/D fixed could appear exactly the same at a single observation time point but could reach their ultimately fatal size in very different lengths of time. This illustrates the clinical difficulty of using only one MRI/CT observation of the lesion and proceeding with treatment without really knowing the expected pattern of growth of the untreated lesion. In Fig. 1 the ratio ρ/D is largest for the solid-like tumor and smallest for the very diffuse tumor. In other words, slowly growing tumors can be very invasive (e.g. gliomatosis cerebri) and very rapidly growing tumors can be solid-like. The key is that the interaction of the growth rate ρ and motility coefficient D are critical in determining the characteristics of the tumor infiltration.

Burgess et al. [16] studied this model in three-spatial dimensions with spherical symmetry and explored the

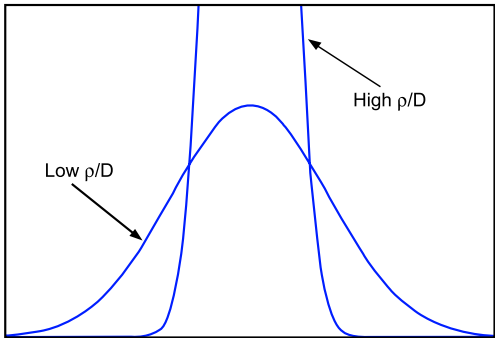

Fig. 1. Cell density profiles for diffuse tumors defined by different values of the ratio of the proliferation rate ρ to the diffusion coefficient D. When ρ/D is large the tumor is predominantly growing so the cell density profile is steep and most of the tumor is detectable by an imaging technique. As ρ/D decreases, the relative contribution of the motility of the cells increases, spreading the cell density profile. The more diffuse tumor is less likely to be accurately identified on medical images.

varied behavior of intermediate-grade gliomas as opposed to high- or low-grade gliomas while ignoring the effects of the brain boundary. They found that there were no mathematical surprises or discontinuities as the continuous variables ρ and D combined in different ways. In addition, they found that highly diffuse intermediate-grade (low ρ, high D) gliomas could have a marginally worse survival time than even high-grade (high ρ, high D) gliomas, suggesting that clinical experiments classifying patients as having "malignant gliomas" might be biologically more heterogeneous than generally considered. In most series, re-evaluations of the histologic appearances of these tumors have indicated that about 80% are glioblastoma and the rest are a variety of other malignant gliomas, so that the biologic variability already has some histologic basis, even disregarding the absence of any actual measures of ρ and D.

To apply the modeling approach to specific patients, a more realistic look at the brain geometry and structure was necessary. The recent model by Swanson et al. [17–22] has introduced the complex geometry of the brain and allowed diffusion (or cell motility) to be a function of the spatial variable $\boldsymbol{x}$ to reflect the observation that glioma cells exhibit higher motility in white matter than in grey matter [23]. The original conservation word equation (1) still applies but the mathematical formulation of the model now written involves spatially varying diffusion, $D(\boldsymbol{x})$,

$$\frac{\partial c}{\partial t} = \nabla \cdot (D(\boldsymbol{x})\nabla c) + \rho c \qquad (3)$$

where $D(\boldsymbol{x}) = D_G$, a constant, for $\boldsymbol{x}$ in grey matter and $D(\boldsymbol{x}) = D_W$, another constant, for $\boldsymbol{x}$ in white matter such that $D_W > D_G$. Estimates of the difference in the diffusion coefficients in grey matter and in white matter have ranged from 2 to 100 fold [17,18].

To accurately analyze the dynamics of this model under the influence of the heterogeneous structure of the human brain, a detailed description of the grey and white matter

distribution throughout the brain was necessary. This was made possible by the neuro-anatomical atlas available on the BrainWeb database [24–26] defining the spatial distribution of grey and white matter throughout the human brain at a resolution of 1 mm^3 voxels.

To relate the velocity v of the detectable tumor margin with the net proliferation rate ρ and a random walk diffusion coefficient D, we use Fisher's approximation: $D = v^2/4\rho$ [6,16]. This approximation comes from the observation that a population governed by growth and diffusion alone expands at a velocity of $2\sqrt{\rho D}$ for large time and is linear for a given ρ and D. The serial CT scans used in the development of the original mathematical model [13] were re-examined to define the rate of advance of the tumor margin within the grey and white matter, v_G and v_W, respectively. Within the tumorous right hemisphere the margin of the detectable tumor moved about 1.5 cm in 180 days [13,15], giving an average velocity of $v = 0.008$ cm/day. For a growth rate $\rho = 0.012$/day, the Fisher approximation then suggests the average diffusion coefficient $D = v^2/4\rho = 0.0013$ cm^2/day. Due to the proximity of this invasion front to the deep cerebral nuclei (predominantly grey matter within the right hemisphere), we associate this value with grey matter diffusion: v_G at 0.008 cm/day [13] and D_G at 0.0013 cm^2/day. From the CT scans, the speed of advance of the tumor margin across the corpus callosum (white matter) is two to three times as fast as that in (predominately) grey matter; thus, we estimate $v_W > 2.2v_G$ at 0.018 cm/day and $D_W > 5D_G$ at 0.0065 cm^2/day.

5. Modeling survival time

To compare with practical clinical measures and to quantify the effectiveness of treatment it was necessary to model the concept of survival time. Analysis of observations of actual patients, living [3,27,28] and dead [29,30], revealed that, although the ranges are wide, gliomas are detectable on enhanced CT at an average diameter of 3 cm (based on a sphere of equal volume to the tumor volume) and fatal at an average diameter of 6 cm. Given estimates of the model parameters for a particular virtual patient, the expected survival time could be calculated as the time it takes for the tumor to grow from 3 to 6 cm in average diameter.

6. Threshold of detection

Since most of the information regarding gliomas of specific patients comes from medical images of various types, it is necessary to translate the model results in terms of their manifestations on CT, MRI, gross and microscopic examinations. These obviously differ, but associated with each imaging technique is a threshold of detection above which the tumor is detectable and below which it is not. For this reason, no presently available medical image will show the entire tumor, including individual cells, because only that portion of the tumor above the threshold of detection will appear on the image. For example, close to the extreme, one 10 μm tumor cell in a pinhead size mass of tissue, say about 1 mm^3, might be cultured in vitro but would require 100 serial sections, each 10 μm thick, to be seen microscopically. To approximate the threshold of detection associated with the detectable boundary of a glioma on enhanced CT, postmortem microscopic analysis of the patient's brain with the treated glioma was compared with the apparent tumor edge defined on enhanced CT, producing an estimate of the threshold of detection on enhanced CT of 400 cells/mm^2 [13]. Note also that 5 cells/mm^2 could perhaps just be recognized at the usual 10 × magnification (which covers about 1 mm^2) but at the next level at magnification (20 ×) would be reduced to about one tumor cell in the field and at the usual high magnification of 40 × would be reduced to one cell in every four fields. This must be close to the threshold detected by microscopists.

7. Model simulations of virtual gliomas

Simulations of virtual gliomas defined by Eq. (3) are given on three different planes (coronal, sagittal, and axial) in Fig. 2. The simulations are presented as contour plots of the tumor cell density: bright red for high density and blue for low, superimposed on a background of grey and white matter provided by the BrainWeb database. The left column of images relates to the time at diagnosis, the enhanced MRI-detectable volume being equivalent to a sphere with a diameter of 3 cm, and the right column to the time at death, the enhanced MRI-detectable area being equivalent to a sphere with a diameter of 6 cm. The thick black curve marks the portion of the tumor detectable on enhanced MRI (400 cells/mm^2) whereas the dark blue contour corresponds to the portion of tumor detectable by a still-theoretical imaging technique with a threshold of detection 80 times more sensitive than enhanced MRI (5 cells/mm^2), but still not zero. Note the striking difference between the enhanced MRI-detectable portion of the tumor and that predicted by the very sensitive theoretical imaging technique, both at the time of diagnosis (left column) and at the time of death (right column).

With this model formulation, a more detailed comparison between actual patient data (CT, MRI, gross and microscopic) is possible. That is, given the medical images of the tumor, this model can suggest where the undetectable portion of the tumor may have invaded and at what concentration. This insight might be helpful in defining the best course of treatment for a specific patient; it would certainly be helpful to the pathologist in defining where the tumor might be, at the same time reminding both pathologists and clinicians how far above zero concentra-

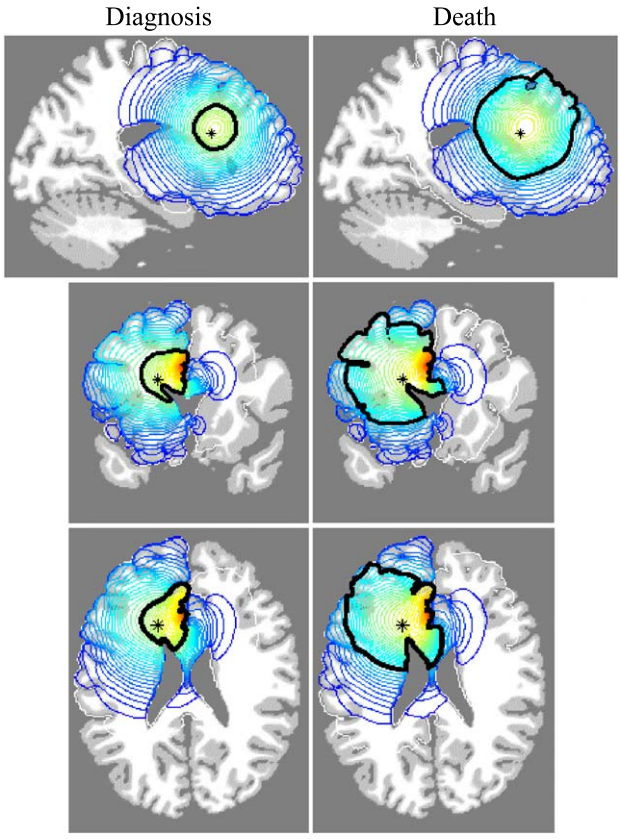

Fig. 2. Sections of a virtual human brain in sagittal, coronal and horizontal planes that intersect at the site of a glioma originating in the superior frontal region denoted by an asterisk (*). The left column of brain sections corresponds to the tumor at diagnosis (3 cm in average diameter) whereas the right column represents the same tumor at death (6 cm in average diameter). Red denotes a high density of tumor cells while blue denotes a low density. A thick black contour defines the edge of the tumor detectable by enhanced MRI. Cell migration was allowed to occur in a truly three-dimensional solid representation of the brain. The elapsed time between diagnosis and death for this virtual glioma is approximately 158 days, about one-fourth of the total history of the tumor. Reprinted from Swanson et al. [22], with the kind permission of Nature Publishing Group.

tion of tumor cells a "negative" microscopic appearance really is.

8. Modeling chemotherapy: polyclonality and heterogeneous drug delivery

Since an untreated patient could only recently be found [19], a treated patient was found with a satisfactorily long course that allowed not only obtaining realistic parameter estimates for that patient but also expanding the model to allow for chemotherapy [13].

Serial CT scans were obtained during the terminal 12 months of a patient with recurrent anaplastic astrocytoma diagnosed and treated at the University of Washington Medical Center, Seattle, WA. During this time, the patient received two different chemotherapies, the first (Course A) consisting of five treatments of a six-drug protocol (6-thioguanine, procarbazine, dibromodulcitol, CCNN, 5-fluorouracil, and hydroxyurea). Each course of treatment was given over 15 days and separated by 6–8 weeks to allow for regeneration of the bone marrow. Following five cycles of the six-drug treatments, the patient received two courses of cysplatinum chemotherapy (Course B) and then, with evidence of additional tumor growth, neutron beam irradiation was given for the last 3 weeks of life, as shown in Fig. 3.

Cruywagen et al. [14] and Tracqui et al. [13] incorporated chemotherapy into the spatially homogeneous model equation (Eq. (1)) by introducing cell death as a loss term. To accommodate this addition, the basic word equation (Eq. (1)) was written as follows:

$$\begin{aligned}&\text{rate of change of tumor cell population}\\&\quad=\text{diffusion (motility) of tumor cells}\\&\qquad+\text{net proliferation of tumor cells}\\&\qquad-\text{loss of tumor cells due to chemotherapy.}\end{aligned}\tag{4}$$

If we let $G(t)$ define the temporal profile of the chemotherapy treatments, then, assuming a loss proportional to the strength or amount of therapy at a given time, the word equation model can be written mathematically as

$$\frac{\partial c}{\partial t}=\nabla\cdot(D\nabla c)+\rho c-G(t)c\tag{5}$$

In the mathematical model, $G(t)=k$ is constant, when chemotherapy is being administered, and $G(t)=0$ otherwise. Here k is a measure of the effectiveness of the treatment. For a tumor to decrease in size during chemotherapy, k must be larger than the growth rate ρ of the cell population.

The existence of drug-resistant cell subpopulations is common in chemotherapy (and radiation treatment); see, for example, Bradford et al. [31]. Cancerous cells are, by nature, unstable. Therefore, exposure to harsh chemicals (or irradiation) can induce either the desired cell death or an undesired sublethal mutation. In the case of the patient studied by Tracqui et al. [13] and Cruywagen et al. [14], the possibility was considered that the radiation therapy administered three years prior to the chemotherapy may have induced a dynamically distinct subpopulation resistant to the subsequent chemotherapy. However, the results showing that both types of cells otherwise appeared identical suggested that it was the initial exposure to chemotherapy that induced the resistant cell clone. The model developed by Tracqui et al. [13] and Cruywagen et al. [14] included drug-sensitive and drug-resistant tumor cell subpopulations. The primary cell subpopulation (n) was postulated to be sensitive to both chemotherapy courses while a mutant subpopulation (m) was postulated to be resistant to Course A. Indeed, the results revealed that the mutant subpopulation (m) had a growth rate similar to that of the primary tumor cell subpopulation (n), but was less

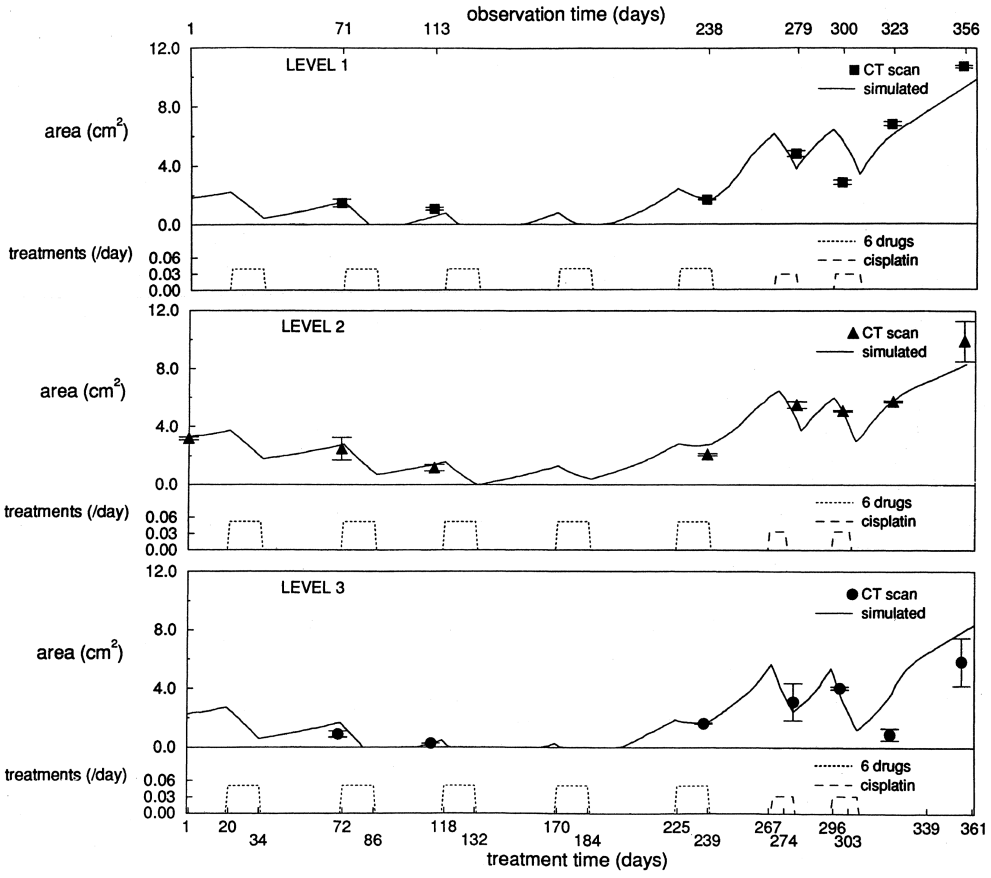

Fig. 3. Tumor area measured at different levels (referred to as levels 1, 2, and 3) of the brain from 8 CT scans taken during the 12 months before the patient's death [13]. During the same terminal year, the patient received five cycles of six drugs (UW protocol) and two cycles of cisplatinum, as indicated, as well as neutron beam irradiation during the last 3 weeks of the patient's life. Simulation of the temporal evolution of the tumor area at each of the brain levels considered. The mathematical model was solved numerically on a two dimensional grid which took into account the meningial and ventricular boundaries at each level. The model calculated effect of chemotherapies on each level is also shown (solid line). Reprinted from Tracqui et al. [13] with the kind permission of Blackwell Sciences.

sensitive to Course B of the chemotherapy than the primary tumor cell subpopulation (n) was to Course A. This indicates that, although the two subpopulations had similar growth characteristics, their sensitivity to the chemotherapies determined the over-all effect. The model showed results in good agreement with the observed CT scan areas (Fig. 3). Thus, the work by Cruywagen et al. [14] and Tracqui et al. [13] strongly suggested that multiple tumor cell subpopulations could be modeled to respond differently to treatment and could be responsible for the treatment failure observed.

A more detailed analysis by Swanson et al. [20] considered chemotherapeutic agents in heterogeneous tissue where drug delivery may vary with vascular density. In regions of grey matter within the brain, where the vasculature is more dense, chemotherapy effectively decreases the rate of tumor growth. However, in white matter regions, drug delivery is ineffective because vascular delivery is significantly less due to the lower vascular density. Swanson et al. [20] discussed a clinical example for which the model-predicted scenario suggested an explanation for the observation of shrinkage of the lesion in certain areas of the brain (grey matter) with continued growth in other areas (white matter).

The recent experimental work on tumor-induced angiogenesis by Folkman [32] led to the development of a variety of models for solid tumor growth including the effects of angiogenesis [33,34]. Chaplain [33] developed models that describe the formation and migratory response of endothelial cells in response to chemical stimuli, i.e. tumor angiogenic factors. Using a discretized form of partial differential equations, theoretical capillary networks similar to experimentally observed structures were produced. From this, the flow of nutrients (such as blood and oxygen) to the tumor, as well as the delivery of chemotherapeutic drugs can be modeled.

El-Kareh and Secomb [35] demonstrated that mathematical models accounting for the kinetics of metabolic and cellular processes can effectively lead to a more rational basis for optimizing the drug administration of chemotherapy treatments. Rather than correlating cell kill with extracellular drug exposure, the kinetics of cell uptake and

metabolism have been examined and cell kill was correlated with a measure of intracellular exposure. Cisplatin was specifically investigated, and data demonstrate that the cell survival fraction correlates better with peak intracellular bound concentration than with other possibilities.

9. Modeling surgical resection

Resection, the surgical removal of an accessible tumor, is a very common treatment for gliomas even though it has shown only limited success. Recurrence of tumor growth at the resection boundary is a well-documented phenomenon [36,37]. Experimentalists and theoreticians alike believe that the distantly invaded cells [5,38] are clearly responsible for tumor reappearance following surgery. The modeling framework suggests that, since the density of cancerous cells remaining after resection is highest at the resection boundary, reappearance at this location seems most likely. That is, the gradient-driven diffusely invasive nature of gliomas is fundamentally responsible for tumor recurrence near the resection boundary.

Isolated glioma cells have been cultured from histologically normal brain over 4 cm from the edge of the bulk tumor [5]. These and other experimental results supporting the very diffuse nature of gliomas have brought about the realization that the trend to extend the range of resection, radiotherapy or other localized treatments is not going to be generally successful. For example, it is fairly common for ^{125}I seeds to be implanted in the grossly normal parenchyma neighboring the resection bed. These seeds are intended to eliminate the diffusely invaded tumor cells at the periphery of the tumor bed. However, mathematical modeling shows that at the time of resection many tumor cells have already migrated not only well beyond the margin of the resection region but also beyond the radiation effects of ^{125}I. Although resection may have succeeded in reducing the pressure effects of the bulk tumor, it is the diffusely invaded tumor cells well beyond the margin that continue to grow and migrate and damage the normal brain parenchyma, ultimately causing death.

Estimating the benefit of surgical resection requires a quantification of the amount of tumor remaining following resection. Alvord [39] assumed that a certain percentage of tumor cells remained after resection and suggested a very simple rule to define the time for the tumor to recur to its mass before surgery: 50% removal required 1 doubling time, 75% removal required two doubling times, 87.5% removal required three doubling times, etc., each halving of the distance to 100% resection providing one additional doubling time. Unfortunately, it required estimation of the classical volume-doubling time, which, as noted in the introduction, is not readily measurable! A more thorough approach was taken by Woodward et al. [15], Cook et al. [40] and Swanson et al. [17,21], who extended the modeling approach described by Tracqui et al. [13] and Cruywagen et al. [14] to consider the effects of surgical resection on glioma recurrence and patient survival.

To simulate surgical resection, the tumor cell density is set to zero inside the resection bed. The basic conservation word equation (Eq. (1)) still applies before and after resection. Three excision diameters were considered: "gross total resection" (3 cm) and "extensive resections" (4 or 5 cm). Death is assumed to occur when the enhanced CT-detectable tumor area equals that of a circle with 6 cm diameter, but the resection bed not only removes some of the concentration gradient driving the cells peripherally but also allows migration back into the resection site. Both increase the duration of survival.

To allow some biological variability in the behavior of high-grade gliomas, Woodward et al. [15] added the assumptions that combinations of variations of 50% above and below the values of ρ and D calculated from the original patient would create nine hypothetical patients (three possible values of ρ combined with three possible values of D) having the appropriate characteristics of a real-life population of patients with high-grade gliomas. Fig. 4 defines the survival time (dotted lines) calculated for the three resection sizes ($S=3$, 4, 5 cm) as well as without resection ($S=0$) for these nine hypothetical patients. The model supports the concept that gliomas infiltrate so diffusely that they cannot be cured by resection alone. Increasing the size of resection does increase life expectancy. There are obvious differences in survival of these hypothetical patients, but how does it relate to real patients?

The availability of results reported by Kreth et al. [37] defining the effectiveness of gross total resection, GTR, as

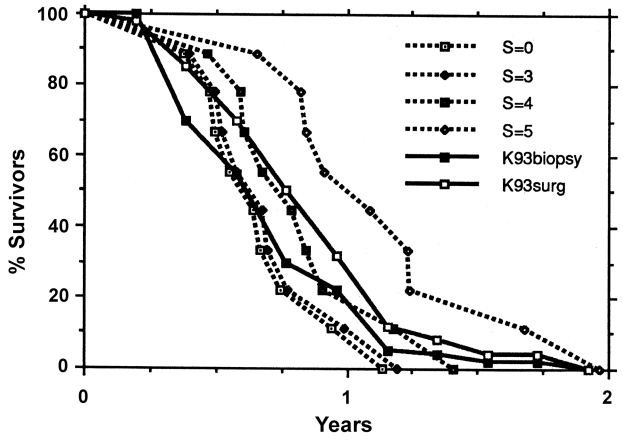

Fig. 4. Superposition of model-simulated survival times (dotted lines) for nine hypothetical patients with high rates of growth and diffusion following varying degrees of resection. The solid lines represent actual survival curves reported by Kreth et al. [37] following biopsy only ('K93biopsy') or extensive surgical resection ('K93surg'); both groups of patients also received post-operative x-irradiation. The median survival times predicted by the model are 33.4 weeks without resection and 35.0, 41.1 and 52.6 weeks with resection as compared to 32 and 39.5 weeks, respectively in reality. Reprinted from Woodward et al. [15] with the kind permission of Blackwell Sciences.

defined by the surgeon, compared to biopsy alone let Woodward et al. [15] compare their model results to actual clinical data. Fig. 4 also shows a superposition of the survival curves found by Kreth et al. [37] (solid lines) on those calculated by Woodward et al. [15] (dotted lines). The agreement between the data sets is remarkable. The model could predit the behavior of gliomas to a degree of accuracy not attainable in vivo with "statistically significant probability" even with groups of over 50 real patients [37]. More recently the results of 70 patients subjected to biopsy, STR or GTR (this time defined by the absence of detectable tumor on post-operative imaging) have been analyzed [41,42]. There was no difference between the survival curves of the biopsy and STR and both approximated the biopsy results of Kreth et al. [37] and the model's results without resection; but the results following GTR [42] were even better than those of Kreth et al. [37], reflecting the more extensive resection documented by post operative imaging.

The model firmly supports the concept that gliomas infiltrate so extensively that they cannot be cured by resection alone. Increasing the size of the resection does increase life expectancy but relatively little. Besides the minimal increase in life expectancy, the model has made no effort to differentiate eloquent regions of the brain that must be spared during such surgical procedures. The theoretical analysis combined with the reality of human brain surgery suggests that resection can never be the sole solution to the treatment of these lesions.

10. Extension to lower grade gliomas

Up to this point the focus of the model has been on high-grade virtual gliomas. Woodward et al. [15] found that allowing the growth rate and the diffusion coefficient D to vary by a factor of 10 simulated well the range of survivals of patients with low- to high-grade gliomas. The 10-fold variations in ρ and D allowed for the representation of four distinct tumor grades: high-grade (high ρ and high D), two intermediate-grades (high ρ and low D or low ρ and high D), and low-grade (low ρ and low D). Although the overall pattern of growth is similar for each of the tumor grades, there are major differences in the time scales: low-grade tumors are generally associated with much longer survival times (years) than high-grade gliomas (months).

Recent extension to actual low-grade lesions was made possible by a study by Mandonnet et al. [43,44] who analyzed a set of 27 untreated lesions (WHO Grade 2 gliomas), mostly oligodendrogliomas, followed with serial imaging without treatment. Recalling Fisher's approximation of a linear progression of the mean radius (or diameter) of the lesion for long times, Mandonnet et al. [43,44] found that the mean diameter of low-grade gliomas does, in fact, fit a linear growth pattern on serial MR imaging: 4.1 mm/year (95% CI: 3.8–4.4 mm/year) (Fig. 5). Fig. 5 also shows,

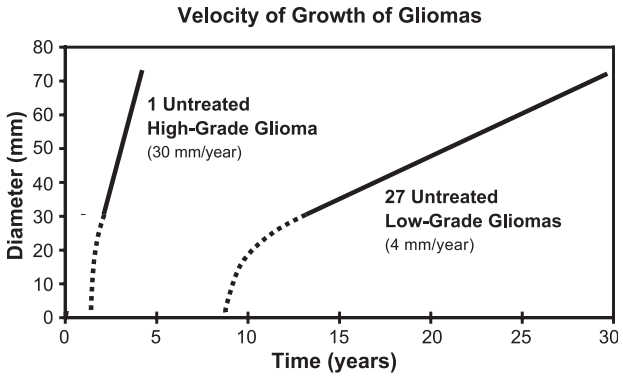

Fig. 5. Velocity of increasing diameter of an untreated glioblastoma [19] and of the average of 27 untreated low-grade gliomas [43,44] detected on MRI, adapted from Shaw and Alvord [50]. Note that both types of lesion have a long silent phase (diameter equals 0) for which they are not detectable by standard imaging—about 1 year for the high-grade lesion and 9 years for the low-grade lesions. After this silent phase, the dotted portion of the curves represent the growth of the lesion before it becomes a clinically detectable size (3 cm in average diameter).

for contrast, the temporal progression of an untreated glioblastoma, a very rare opportunity afforded by a patient who had repeated CT/MRI examinations without intervening treatment [19]. As Woodward et al. [15] predicted, this velocity is approximately 10 times that of the low-grade: 30 mm/year. It should be noted that the linearity for both low- and high-grade gliomas is true only after a long period of time, but this is typical of the clinically detectable part of the life histories of the gliomas, as also indicated in Fig. 5.

The observations of some pediatric low-grade astrocytomas led Lazareff et al. [45,46] to conclude that at a particular volume (approximately 100–150 cm^3) tumor growth may cease. A similar gompertzian growth pattern for optic gliomas was suggested by Alvord and Lofton [46] and Alvord [47]. A more specific mathematical model was developed by Newman and Lazareff [48] involving the interaction of promoters and inhibitors in the growth of these lesions.

11. Discussion

In this review we have briefly described the evolution of mathematical models for glioma growth and invasion beginning in simple homogeneous tissue, with or without gross anatomical boundaries (skull and ventricles), extending to complex heterogeneous tissue, with varying proportions of grey and white matter in cerebral cortex (including the sulcal pattern), deep cerebral nuclei, brainstem and cerebellum. These models have been based on "thresholds of detection" on currently available scans (CT and MRI) to describe and quantify the diffusive nature of gliomas by isolating characteristics such as the effect of the ratio ρ/D of the proliferation rate ρ to the diffusion rate D in defining the spatial temporal pattern of tumorous growth.

Other factors considered include the effect of chemotherapy and surgical resection, the differences between high- and low-grade gliomas (especially with two types of intermediate-grade gliomas, one with a prognosis even worse than the high-grade).

Such realistic mathematical modeling has been helpful in highlighting and demonstrating the fact that any local treatment of a diffusely invading glioma will fail. Mathematical modeling can be critical in deducing the extent of sub-microscopic spread of the tumor and thus in determining the locations of active invasion of the tumor. Whether this will help localize treatment remains doubtful, however, since the invasion is most likely still more peripheral than any localizable treatment can reach. The model predicts that gliomas can be modeled as traveling waves with diameter increasing linearly with time, and this has been proven in a series of untreated low-grade gliomas [43,44] and one untreated glioblastoma [19]. The model can probably be expanded to consider the effects of other factors, such as edema in mediating diffusion (migration), but its main thrust may be to see if simultaneous CT and MRI scans, such as Kelly et al. [28] accomplished, provide enough information to define ρ and D in individual patients at one point in time. If so, it may at long last be possible to estimate the prognosis for individual patients and to provide much more homogeneous populations of patients for clinical trials. Although the model predicts the average and the shape of the survival curve of groups of patients, it is more likely that two sets of scans without intervening treatment will be necessary to define ρ and D accurately enough to predict the prognosis for individual patients.

As noted in Introduction, mathematical modeling is dictated by the biology and not the mathematics [6]. We have attempted to analyze the behavior of gliomas mechanistically, deriving their behavior from two fundamental properties, ρ and D. Although these clearly determine the tumor's growth as an expansion of its traveling wave front, other factors combine to determine the patient's prognosis, the survival time. The most prominent of the other factors, age and Karnofsky performance score (KPS), correlate well with prognosis but are stochastic phenomena that currently have no underlying mechanisms that are understood well enough to be incorporated in the model. Thus, in terms of prognosis the model considers ''ideal'' patients unencumbered by high age and low KPS [49] that prevent such patients from reaching their predicted survival time.

Acknowledgements

KRS acknowledges the support of the Mathematical Biology Training Grant (BIR-9256532 from the U.S. National Science Foundation), the Academic Pathology Fund and the NSF Mathematical Sciences Postdoctoral Fellowship (DMS-9902385). ECA acknowledges the support of Grant number HD-02274 from the National Institutes of Health to the Center on Human Development and Disability.

References

[1] Alvord Jr EC, Shaw CM. Neoplasms affecting the nervous system of the elderly. In: Duckett S, editor. The Pathology of the Aging Human Nervous System. Philadelphia: Lea and Fabiger; 1991. p. 210–86.
[2] Silbergeld DL, Rostomily RC, Alvord Jr EC. The cause of death in patients with glioblastoma is multifactorial: clinical factors and autopsy findings in 117 cases of supratentorial glioblastoma in adults. J Neurol Oncol 1991;10:179–85.
[3] Blankenberg FG, Teplitz RL, Ellis W, Salamat MS, Min BH, Hall L, et al. The influence of volumetric tumor doubling time, DNA ploidy, and histologic grade on the survival of patients with intracranial astrocytomas. AJNR Am J NeuroRad 1995;16:1001–12.
[4] Shuman RM, Alvord Jr EC, Leech RW. The biology of childhood ependymomas. Arch Neurol 1975;32:731–9.
[5] Silbergeld DL, Chicoine MR. Isolation and characterization of human malignant glioma cells from histologically normal brain. J Neurosurg 1997;86:525–31.
[6] Murray JD. Mathematical Biology. 3rd ed. New York, NY: Springer-Verlag; 2002.
[7] Collins VP, Loeffler RK, Tivey H. Observations on growth rates of human tumors. Am J Roetgenol Radium Ther Nucl Med 1956; 76:988–1000.
[8] Kusama S, Spratt Jr JS, Donegan WL, Watson FR, Cunningham C. The gross rates of growth of human mammary cancer. Cancer 1972;30:594–9.
[9] Mayneord WV. On the law of growth in Jensen's rat sarcoma. Am J Cancer 1932;16:841–6.
[10] Alvord Jr EC. Hypothesis: growth rates of epidermoid tumors. Ann Neurol 1977;2:367–70.
[11] Deisboeck T. Pattern of self-organization in tumor systems: complex growth dynamics in a novel brain tumor spheroid model. Cell Prolif 2001;34:115–34.
[12] Steel GG. Growth Kinetics of Tumors. Cell Population Kinetics in Relation to the Growth and Treatment of Cancer. Oxford: Clarendon Press; 1977.
[13] Tracqui P, Cruywagen GC, Woodward DE, Bartoo GT, Murray JD, Alvord Jr EC. A mathematical model of glioma growth: the effect of chemotherapy on spatio-temporal growth. Cell Prolif 1995;28: 17–31.
[14] Cruywagen GC, Woodward DE, Tracqui P, Bartoo GT, Murray JD, Alvord Jr EC. The modeling of diffusive tumors. J Biol Syst 1995;3: 937–45.
[15] Woodward DE, Cook J, Tracqui P, Cruywagen GC, Murray JD, Alvord Jr EC. A mathematical model of glioma growth: the effect of extent of surgical resection. Cell Prolif 1996;29:269–88.
[16] Burgess PK, Kulesa PM, Murray JD, Alvord Jr EC. The interaction of growth rates and diffusion coefficients in a three-dimensional mathematical model of gliomas. J Neuropathol Exp Neurol 1997; 56:704–13.
[17] Swanson KR, Mathematical Modeling of the Growth and Control of Tumors. PhD thesis. University of Washington; 1999.
[18] Swanson KR, Alvord Jr EC, Murray JD. A quantitative model for differential motility of gliomas in grey and white matter. Cell Prolif 2000:317–30.
[19] Swanson KR, Alvord Jr EC. A biomathematical and pathological analysis of an untreated glioblastoma. 7th European Congress of Neuropathology (Helsinki, Finland); 2002 p. 28.
[20] Swanson KR, Alvord Jr EC, Murray JD. Quantifying efficacy of chemotherapy of brain tumors (gliomas) with homogeneous and heterogeneous drug delivery. Acta Biotheor 2002;50:223–37.

[21] Swanson KR, Alvord Jr EC, Murray JD. Virtual resection of gliomas: effects of location and extent of resection on recurrence. Math Comput Model 2003 [in press].
[22] Swanson KR, Alvord Jr EC, Murray JD. Virtual brain tumors (gliomas) enhance the reality of medical imaging and highlight inadequacies of current therapy. Br J Can 2002;86:14–8.
[23] Giese A, Kluwe L, Laube B, Meissner H, Berens M, Westphal M. Migration of human glioma cells on myelin. Neurosurgery 1996;38: 755–64.
[24] Kwan R, Evans AC, Pike GB. An extensible MRI simulator for post-processing evaluation. Procedings of the 4th international conference on visualization in biomedical computing, vol. 96. 1996. p. 135–40.
[25] Cocosco CA, Kollokian V, Kwan RKS, Evans AC. Brainweb: online interface to a 3D MRI simulated brain database. Neuroimage 1997; 5:S425.
[26] Collins DL, Zijdenbos AP, Kollokian V, Sled JG, Kabani NJ, Holmes CJ, et al. Design and construction of a realistic digital brain phantom. IEEE Trans Med Imag 1998;17:463–8.
[27] Shrieve DC, Alexander III E, Wen PY, Kooy HM, Black PM, Loeffler JS. Comparison of sterotactic radiosurgery and brachytherapy in the treatment of recurrent glioblastoma multiforme. Neurosurgery 1995;36:275–82.
[28] Kelly PJ, Daumas-Duport C, Kispert DB, Kall BA, Scheithaurer BW, Illig JJ. Imaging-based sterotaxic serial biopsies in untreated intracranial glial neoplasms. J Neurosurg 1987;66:865–74.
[29] Burger PC, Heinz ER, Shibata T, Kleihues P. Topographic anatomy and CT correlations in the untreated glioblastoma multiforme. J Neurosurg 1988;68:698–704.
[30] Concannon JC, Kramer S, Berry R. The extent of intracranial gliomata at autopsy and its relation to techniques used in radiation therapy of brain tumors. Am J Roentgenol Radium Ther Nucl Med 1960; 84:99–107.
[31] Bradford R, Koppel H, Pilkington GJ, Thomas DG, Darling JL. Heterogeneity of chemosensitivity in six clonal cell lines derived from a spontaneous murine astrocytoma and its relationship to genotypic and phenotypic characteristics. J Neurol Oncol 1997;34:247–61.
[32] Folkman J. Angiogenesis in cancer, vascular, rheumatoid and other diseases. Nat Med 1995;1:27–31.
[33] Chaplain M. Mathematical modelling of angiogenesis. J Neurol Oncol 2000;50:37–51.
[34] McDougall SR, Anderson ARA, Chaplain MAJ, Sherratt JA. Mathematical modelling of flow through vascular networks: implications for tumor-induced angiogenesis and chemotherapy strategies. Bull Math Biol 2002;64:673–702.
[35] El-Kareh A, Secomb TW. A mathematical model for comparison of bolus injection, continuous infusion, and liposomal delivery of doxorubicin to tumor cells. Neoplasia 2000;2:325–38.
[36] Kelly PJ, Hunt C. The limited value of cytoreductive surgery in elderly patients with malignant gliomas. Neurosurgery 1994;34: 62–7.
[37] Kreth FW, Warnke PC, Scheremet R, Ostertag CB. Surgical resection and radiation therapy versus biopsy and radiation therapy in the treatment of glioblastoma multiforme. J Neurosurg 1993;78:762–6.
[38] Chicoine MR, Silbergeld DL. Assesment of brain tumor cell motility in vivo and in vitro. J Neurosurg 1995;82:615–22.
[39] Alvord Jr EC. Simple model of recurrent gliomas. J Neurosurg 1991;75:337–8.
[40] Cook J, Woodward DE, Tracqui P, Cruywagen GC, Murray JD, Bartoo GT, et al. Resection of gliomas and life expectancy. J Neurol Oncol 1995;24:131.
[41] Kennedy G, Rizvi A, Goodkin R, Barber J, Ojemann G, Winn HR, et al. Pre-operative MRI imaging characteristics and tumor volumes and outcome for adult patients with previously untreated glioblastomas. Neurol Oncol 2001;3:343–4.
[42] Swanson KR, Alvord Jr EC, Rostomily R. 3D quantitative modeling of gliomas growth and invasion: predictions of survival time from imaging characteristics. 5th conference of the European society of the mathematical and theoretical biology, Milano, Italy 2002:136.
[43] Mandonnet E, Broët P, Swanson KR, Carpentier A, Delattre JY, Capelle L. Linear growth of mean tumor diameter in low grade gliomas. Neurology 2002;58(Suppl. 3):A13.
[44] Mandonnet E, Delattre JY, Tanguy ML, Swanson KR, Carpentier AF, Duffau H, et al. Continuous growth of mean tumor diameter in a subset of WHO grade II gliomas. Ann Neurol 2003;53:524–8.
[45] Lazareff JA, Suwinski R, De Rosa R, Olmstead CE. Tumor volume and growth kinetics in hypothalamic–chiasmatic pediatric low-grade gliomas. Pediatr Neurosurg 1999:312–9.
[46] Alvord Jr EC, Lofton S. Gliomas of the optic nerve or chiasm: outcome by patients' age, tumor site, and treatment. J Neurosurg 1988; 68:85–98.
[47] Alvord Jr EC. Growth rates in optic gliomas. Optic gliomas in neurofibromatosis, vol. 2. New York: National Neurofibromatosis Foundation; 1989. p. 99–119.
[48] Newman W, Lazareff J. A mathematical model for self-limiting tumors. J Theor Biol: 2003;222:361–71.
[49] Lacroix M, Abi-Said D, Fourney DR, Gokaslan ZL, Shi WM, DeMonte F, et al. A multivariate analysis of 416 patients with glioblastoma multiforme: prognosis, extent of resection, and survival. J Neurosurg 2001;95:190–8.
[50] Shaw CM, Alvord Jr EC. Investigations: neuropathology. In: Moore AJ, Newell DW, editors. Interventional neurosurgical practices. London: Springer-Verlag; 2003. In Press.